Up and down the Riemann surfaces of the Λ baryon form factors

Simone Pacetti[1,2,*], *Egle* Tomasi-Gustafsson[3,**], *Alessio* Mangoni[1], and *Olga* Shekhovtsova[2,***]

[1]Dipartimento di Fisica e Geologia, 06123 Perugia, Italy
[2]INFN Sezione di Perugia, 06123 Perugia, Italy
[3]DPhN, IRFU, CEA, Université Paris-Saclay, 91191 Gif-sur-Yvette Cedex, France

Abstract. The recent measurement of the modulus and phase of the ratio G_E^Λ/G_M^Λ, between the electric and the magnetic Λ form factors, performed by the BESIII experiment, offers the unique possibility of exploring for the first time ever the complex structure of this form factor ratio. The investigation is made possible by a dispersive procedure based on analyticity and a set of first-principle constraints, that is defined ad hoc.

1 Introduction

The four-current associated with a baryon-baryon-photon vertex is parametrized by two independent Lorentz scalar functions of q^2, being q the four-momentum of the photon.They are called form factors (FFs) and are not constant because baryons have a composite structure. Among the infinite possible choices, the most commonly used are the so-called Sachs electric and magnetic FFs, G_E and G_M [1]. These FFs have the peculiarity of representing the Fourier transforms of the electric and magnetic-momentum spatial densities in the non-relativistic limit, e.g. in the reference system, called Breit frame, where the energy component of the photon four-momentum vanishes so that $q = (0, \vec{q})$. Analyticity and unitarity define the reality domain of FFs in the q^2-complex plane. For real values of q^2, and hence for physical four-momenta q, FFs are real in the whole space-like region, $q^2 < 0$, and in portion of the time-like interval below the theoretical threshold $q^2_{\rm th} = (2M_\pi)^2$, while they have a non-vanishing imaginary part above this threshold. Such a threshold corresponds to the mass squared of the lightest hadronic channel, the $\pi^+\pi^-$ one, that, having the same quantum numbers of the virtual photon, can couple to it.

2 The peculiar case of the Λ baryon

The Λ baryon, and hence the $\Lambda\bar{\Lambda}$ system produced in e^+e^- annihilation reactions, has isospin zero, then its theoretical threshold is $q^2_{\rm th} = (2M_\pi + M_{\pi^0})^2$, where M_π and M_{π^0} are the charged and neutral pion mass, respectively. Indeed, the lightest hadronic, isoscalar state that can couple to the $\Lambda\bar{\Lambda}$ final state is that of three pions: $\pi^+\pi^-\pi^0$.

*e-mail: simone.pacetti@unipg.it
**e-mail: egle.tomasi@cea.fr
***e-mail: olga.shekhovtsova@pg.infn.it

© The Authors, published by EDP Sciences. This is an open access article distributed under the terms of the Creative Commons Attribution License 4.0 (https://creativecommons.org/licenses/by/4.0/).

2.1 The experimental accessibility

Even in an ideal laboratory with no experimental limitations, FFs would not be fully measurable over the entire kinematic region corresponding to all space-like and time-like transferred four-momentum q, i.e., for $q^2 \in (-\infty, +\infty)$. Form factors' values at different energies are extracted from observables related to reactions occurring in specific kinematic domains.

1. In the space-like region, $q^2 \leq 0$, electric and magnetic Λ FFs, G_E^Λ and G_M^Λ are real and their values should be extracted from the differential cross section of the elastic scattering reaction $e^-\Lambda \to e^-\Lambda$.

2. In the time-like domain, $q^2 \geq q^2_{\rm phy}$, where $q^2_{\rm phy} = (2M_\Lambda)^2$ is the physical production threshold, FFs have a non-zero imaginary part and from the differential cross section of the annihilation process $e^+e^- \to \Lambda\bar{\Lambda}$, only the moduli of FFs can be extracted.

3. The FF values for $q^2 \in \left(q^2_{\rm th}, q^2_{\rm phy}\right)$ can be extracted from the differential cross section of the reaction $\Lambda\bar{\Lambda} \to \eta e^+e^-$, with the pseudo-scalar meson η emitted by one of the initial baryons. The idea of using this reaction is inspired by the works reported in Refs. [2, 3], where the approach is discussed for the homologous reaction $p\bar{p} \to \pi^0 e^+e^-$.

The measurements described at points one and three, used to extract FF values in the space-like and unphysical regions, are, at present, not doable due to the technical impossibility of realizing either stable targets or stable beams of Λ baryons. Nevertheless, in the case of the Λ baryon, the lack of experimental information is compensated by the unique opportunity of exploiting the self-analyzing power of the weak decay $\Lambda \to p\pi^-$, which is commonly used to identify the Λ baryon and to the measure its polarization, which is extracted from the angular distribution of the final proton. This gives the opportunity to access the relative phase $\arg\left(G_E^\Lambda/G_M^\Lambda\right)$ without requiring a direct polarization measurement, which needs adding a polarimeter to the main detector.

3 Polarization observables and data

The complex nature of FFs in the time-like region is a source of polarization for baryons and anti-baryons produced in e^+e^--annihilation reactions [4], even when initial leptons are unpolarized. In fact, the component of the baryon polarization vector along the direction orthogonal to the scattering plane has the expression

$$\mathcal{P}_\perp = -\frac{\sqrt{\tau}\,|G_E|\,/\,|G_M|}{\tau\left(1+\cos^2(\theta)+\sin^2(\theta)\,|G_E|^2\,/\,|G_M|^2\right)}\sin(2\theta)\sin\left(\arg\left(\frac{G_E}{G_M}\right)\right), \quad \tau = \sqrt{\frac{q^2}{4M^2}},$$

where G_E and G_M are the electric and magnetic Sachs FFs of the baryon, M is its mass, q is the momentum transferred and θ the scattering angle in the e^+e^- center-of-mass reference frame, and it does not depend on the polarization of the initial leptons. It is interesting to point out that from the measurement of $\mathcal{P}_\perp$ only the sinus of the relative phase $\arg(G_E/G_M)$ can be obtained. The spin correlation between the baryon and the antibaryon gives, instead, the cosine of $\arg(G_E/G_M)$ [5, 6], so that, the knowledge of both these observables allows us to define the determination of the relative phase. On the other hand, even in this ideal experimental situation the Riemann sheet of the complex ratio G_E/G_M would still be undetermined. This crucial issue will be discussed in the conclusions. Two sets of data on the modulus and phase of the ratio G_E^Λ/G_M^Λ are available from BaBar [7] and BESIII [8] experiments. These data are shown in Fig. 1, where, besides the modulus and the phase, the sinus of the phase, which represents the genuine experimental observable, is also shown.

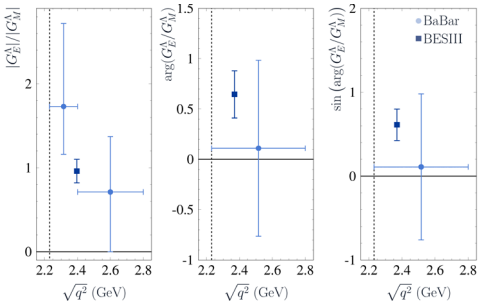

Figure 1. Data on the modulus, left panel; the phase, central panel; the sinus of the phase, right panel, of the ratio G_E^Λ/G_M^Λ measured by BaBar [7], light-blue solid circles, and BESIII [8], dark-blue solid square, experiments.

4 The idea behind the study

The phase $\arg\left(G_E^\Lambda/G_M^\Lambda\right)$, whose determination, as already underlined, is not experimentally accessible, embodies interesting information about the ratio G_E^Λ/G_M^Λ itself as a function of q^2. In particular, assuming that the magnetic FF does not vanish, the time-like asymptotic behavior of $\arg\left(G_E^\Lambda/G_M^\Lambda\right)$ gives, in units of π radians, the number of zeros which the electric FF possesses on the q^2 complex plane. This is the well known thesis of the Levinson's theorem [9]. A procedure based on the dispersion relation for the imaginary part is defined in order to obtain the analytic continuation of the complex function G_E^Λ/G_M^Λ in the whole q^2-complex plane. The main ingredient is a suitable parametrization of the imaginary part $\mathrm{Im}\left(G_E^\Lambda/G_M^\Lambda\right)$ only in the portion $(q^2_{\rm th}, q^2_{\rm asy})$ of the upper edge of the time-like cut $(q^2_{\rm th}, \infty)$, where it is different from zero, being $q^2_{\rm asy}$ the threshold from which the ratio assumes only real values as a consequence of the Phragmén-Lindelöf theorem [10]. The imaginary part is parametrized by a combination of Chebyshev polynomials [11]

$$\mathrm{Im}\left(\frac{G_E^\Lambda(q^2)}{G_M^\Lambda(q^2)}\right) \equiv Y\left(q^2;\vec{C},q^2_{\rm asy}\right) = \begin{cases} \sum_{j=0}^{N} C_j T_j\left[x\left(q^2\right)\right] & q^2_{\rm th} < q^2 < q^2_{\rm asy} \\ 0 & \text{elsewhere} \end{cases},$$

where $\vec{C} \in \mathbb{R}^{N+1}$ is the coefficients vector, $\left\{T_j(x)\right\}_{j=0}^{N}$ is the set on the first $(N+1)$ Chebyshev polynomials and $x\left(q^2\right) = 2\left(q^2 - q^2_{\rm th}\right)/\left(q^2_{\rm asy} - q^2_{\rm th}\right) - 1$ is the change of variable which translates the q^2 interval $[q^2_{\rm th}, q^2_{\rm asy}]$ to the one defined for Chebyshev polynomials, i.e., $[-1, 1]$. The set of $(N+2)$ free parameters $\left\{\vec{C} = (C_0, C_1, \ldots, C_N), q^2_{\rm asy}\right\}$ of the function Y is determined by imposing directly and through dispersion relations theoretical and experimental constraints. Three theoretical constraints are imposed directly on $Y\left(q^2;\vec{C},q^2_{\rm asy}\right)$ at the thresholds: $q^2_{\rm th}$, $q^2_{\rm phy}$ and $q^2_{\rm asy}$, where the ratio G_E^Λ/G_M^Λ is real and hence the imaginary part vanishes. Other theoretical and experimental conditions concern the modulus, the phase, and the real part of G_E^Λ/G_M^Λ. In order to implement them, it needs the parametrization of the real part, which can be obtained as the analytic continuation of that for the imaginary part through the following dispersion relation

$$\mathrm{Re}\left(\frac{G_E^\Lambda(q^2)}{G_M^\Lambda(q^2)}\right) \equiv X\left(q^2;\vec{C},q^2_{\rm asy}\right) = \frac{q^2}{\pi}\,\mathrm{Pr}\int_{q^2_{\rm th}}^{q^2_{\rm asy}} \frac{Y\left(s;\vec{C},q^2_{\rm asy}\right)}{s(s-q^2)}ds\,.$$

The χ^2 is defined as: $\chi^2\left(\vec{C}',q^2_{\rm asy}\right) = \chi^2_{\rm abs} + \chi^2_{\rm phase} + \tau_{\rm phy}\chi^2_{\rm phy} + \tau_{\rm asy}\chi^2_{\rm asy} + \tau_{\rm curv}\chi^2_{\rm curv}$, where the parameter vector $\vec{C}' = (C_3, C_4, \ldots, C_N)$ has only the last $(N-2)$ components of the original $\vec{C}$, since the first three coefficients C_0, C_1 and C_2 are fixed by imposing the three

nodes for the imaginary part at the three thresholds, i.e., $Y\left(q^2_{\rm th},\vec{C},q^2_{\rm asy}\right) = Y\left(q^2_{\rm phy},\vec{C},q^2_{\rm asy}\right) = Y\left(q^2_{\rm asy},\vec{C},q^2_{\rm asy}\right) = 0$. The first two contributions are the experimental constraints for the modulus and the phase of the ratio

$$\chi^2_{\rm abs} = \sum_{j=1}^{M}\left(\sqrt{X^2\left(q^2_j\right)+Y^2\left(q^2_j\right)} - |G^\Lambda_E/G^\Lambda_M|_j\right)^2 / \left(\delta|G^\Lambda_E/G^\Lambda_M|_j\right)^2 ,$$

$$\chi^2_{\rm phase} = \sum_{k=1}^{P}\left(\sin\left(\arctan\left(Y\left(q^2_k\right)/X\left(q^2_k\right)\right)\right) - \sin\left(\arg\left(G^\Lambda_E/G^\Lambda_M\right)_k\right)\right)^2 / \left(\delta\arg\left(G^\Lambda_E/G^\Lambda_M\right)_k\right)^2 ,$$

where $\left\{q^2_j, |G^\Lambda_E/G^\Lambda_M|_j, \delta|G^\Lambda_E/G^\Lambda_M|_j\right\}_{j=1}^{M}$ and $\left\{q^2_k, \arg(G^\Lambda_E/G^\Lambda_M)_k, \delta\arg(G^\Lambda_E/G^\Lambda_M)_k\right\}_{k=1}^{P}$ are the corresponding data sets. The second pair $\chi^2_{\rm phy} = \left(1 - X\left(q^2_{\rm phy};\vec{C}',q^2_{\rm asy}\right)\right)^2$ and $\chi^2_{\rm asy} = \left(1 - X^2\left(q^2_{\rm asy};\vec{C}',q^2_{\rm asy}\right)\right)^2$, which are forced to be exactly satisfied by means of the weighting factors $\tau_{\rm phy}$ and $\tau_{\rm asy}$, are for the theoretical conditions at the physical and asymptotic thresholds. The last contribution

$$\chi^2_{\rm curv} = \int_{q^2_{\rm th}}^{q^2_{\rm asy}} \left|d^2Y\left(s;\vec{C}',q^2_{\rm asy}\right)/ds^2\right|^2 ds$$

represents the total curvature of the imaginary part, suitably weighted by $\tau_{\rm curv}$, and regularizes the solutions [12]. The real time-like asymptotic behavior of the ratio is left free by setting $\tau_{\rm asy} = 0$. The constraint at the physical threshold is required by setting $\tau_{\rm phy}$ higher enough to cancel the corresponding contribution $\chi^2_{\rm phy}$. The calibration of the regularization factor $\tau_{\rm curv}$ is made [13] by studying the behaviors of χ^2 and $q^2_{\rm asy}$ as functions of $\tau_{\rm curv}$ itself and of the number $N+1$ of the considered Chebyshev polynomials. In particular, a compromise is found between high values, which suppress physical oscillations and give almost flat solutions, and low values, which, instead, allow unphysical fluctuations.

5 Results

In order to estimate the errors, a Monte Carlo method is adopted. It consists of analyzing with the standard statistical techniques the set of results obtained by repeating the minimization procedure on a certain number R of data sets generated by normal random fluctuations of the original ones. Each solution, i.e., each set of parameters $\left\{\vec{C}',q^2_{\rm asy}\right\}$ is classified in terms of the two positive or negative integers numbers: $N_{\rm th} = \arg\left(G^\Lambda_E(q^2_{\rm th})/G^\Lambda_M(q^2_{\rm th})\right)/\pi$, $N_{\rm asy} = \arg\left(G^\Lambda_E(q^2_{\rm asy})/G^\Lambda_M(q^2_{\rm asy})\right)/\pi$, representing, in units of π radians, the phase of the FFs ratio at the theoretical and asymptotic thresholds. They are positive or negative integers since the function G^Λ_E/G^Λ_M is real at these thresholds, and they are not simply zero because the ratio can assume values on different Riemann surfaces, not only on the fundamental one. The results are reported in Table 1. The eight combinations of $(N_{\rm th}, N_{\rm asy})$ are listed with the corresponding fractions, which can be interpreted as occurrence probabilities. We accept only the six results with a probability larger than 0.5%. The fact that so few cases are selected, despite the lack of data, proves the strength and effectiveness of the theoretical frame of the procedure. At the theoretical threshold the phase can assume three possible values: 0 or $\pm\pi$, i.e., $N_{\rm th} = 0$ or $N_{\rm th} = \pm 1$. This apparently strange values for a real quantity have a quite simple explanation in terms of the signs of the FFs G^Λ_E and G^Λ_M just below the theoretical threshold $q^2_{\rm th}$.

Concerning the asymptotic behavior, the FF ratio is assumed to be real starting from $q^2_{\rm asy}$ up

$N_{\rm th}$	$N_{\rm asy}$	%	Visual percentage
-1	0	4.0	
-1	1	16.0	
-1	2	50.5	
-1	3	0.7	
0	1	0.3	
0	3	26.8	
1	2	0.1	
1	3	1.6	

Table 1. Numerical and visual percentage of cases corresponding to the values of the phase, in units of π radians, at $q^2_{\rm th}$ and $q^2_{\rm asy}$.

to infinity. As a consequence, the phase in this q^2 region is constant and equal to $N_{\rm asy}\pi$. Moreover, assuming no zeros in the q^2-complex plane with the branch cut $(q^2_{\rm th}, \infty)$ for the magnetic FF, the ratio is analytic in the same domain. From the Levinson's theorem it follows that $N_{\rm asy}$ is greater than $N_{\rm th}$. In fact, because of the normalization $G^\Lambda_E(0) = 0$, $N_{\rm asy} \geq N_{\rm th} + 1$. The six double graphs of Fig. 2 show the obtained error bands for moduli and phases of the ratio, for the six pairs of $(N_{\rm th}, N_{\rm asy})$ having probability larger than 0.5% (see Table 1). The error bands are determined with the Monte Carlo technique described in the previous section. It is interesting to see how the dispersive procedure assigns different determinations to phase values extracted from the same data. In particular, to the value extracted from the most precise BESIII data, shown as a dark blue square in the right panel of Fig. 1, is assigned the fundamental determination, namely $2k\pi < \arg(G^\Lambda_E/G^\Lambda_M) < (2k + 1/2)\pi$, being $0 < \sin\left(\arg(G^\Lambda_E/G^\Lambda_M)\right) < 1$, with $k \in \mathbb{N} \cup \{0\}$, obtained by the dispersive analysis. The determination of the BaBar point follows as a consequence. As shown in the lower panel of the left-down graph of Fig. 2, only in the case with $(N_{\rm th}, N_{\rm asy}) = (-1, 3)$, where $k = 1$, the two fundamental determinations are different, the BESIII phase lies in $2\pi < \arg(G^\Lambda_E/G^\Lambda_M) < 5\pi/2$, while the BaBar one in $5\pi/2 < \arg(G^\Lambda_E/G^\Lambda_M) < 3\pi$. More in detail, k is zero in the first three cases, with $(N_{\rm th}, N_{\rm asy}) = (-1, 0)$, $(-1, 1)$, $(-1, 2)$, and $k = 1$ for: $(N_{\rm th}, N_{\rm asy}) = (-1, 3)$, $(0, 3)$, $(1, 3)$.

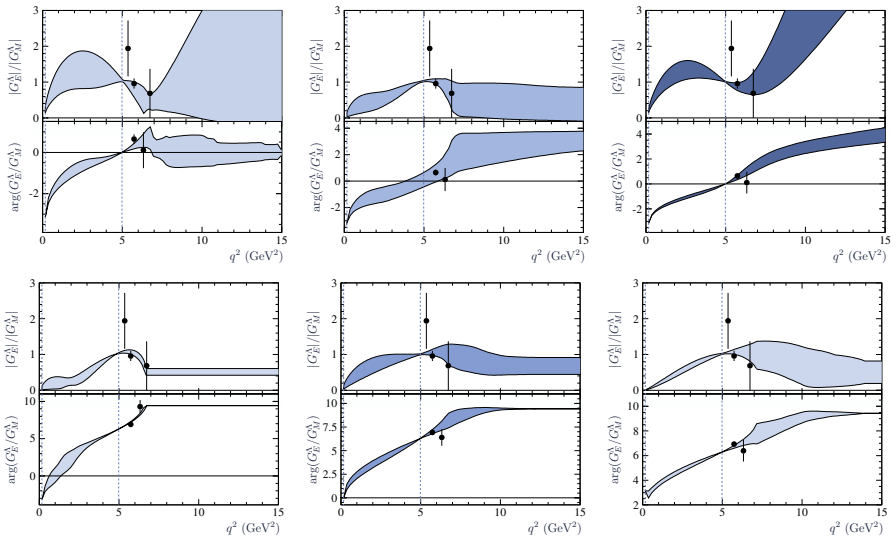

Figure 2. Modulus (upper panels) and phase (lower panels) of the FF ratio with, from the top left to the down right: $(N_{\rm th}, N_{\rm asy}) = (-1, 0), (-1, 1), (-1, 2), (-1, 3), (0, 3), (1, 3)$. The color intensity is proportional to the occurrence probability, a darker color indicates a higher probability.

5.1 The modulus of the ratio

Despite the fact that the modulus of the FF ratio is a well-established observable, in contrast to the phase, whose determination is unknown, the lack of data makes predictions quite uncertain, especially for the high-q^2 behavior. The obtained asymptotic thresholds $\left(q^2_{\rm asy} \pm \delta q^2_{\rm asy}\right)$, as well as the corresponding values of the modulus of the ratio $\left(R_{\rm asy} \pm \delta R_{\rm asy}\right)$, where $R_{\rm asy}$ is defined as $R_{\rm asy} \equiv |G_E^\Lambda(q^2_{\rm asy})/G_M^\Lambda(q^2_{\rm asy})|$, are reported in Fig. 3. The ellipses are centered at $(q^2_{\rm asy}, R_{\rm asy})$ and have as horizontal and vertical semi-axes the uncertainties $\delta q^2_{\rm asy}$ and $\delta R_{\rm asy}$, respectively. Their large errors do not allow any precise prediction. It is interesting to notice how the convergence $|G_E^\Lambda(q^2)| \to |G_M^\Lambda(q^2)|$ as $q^2 \to \infty$ is compatible with any case, but for that with $(N_{\rm th}, N_{\rm asy}) = (-1, 2)$, described by the darker blue band in Figs. 2 and 3, which is the most probable one, see Table 1. So that, the knowledge of the modulus of the ratio at higher time-like q^2 would play a key role in establishing the phase determination and hence in giving a hint on the pair $(N_{\rm th}, N_{\rm asy})$ that describes the phase evolution with q^2 only in the case of $R_{\rm asy} > 6$ implying $(N_{\rm th}, N_{\rm asy}) = (-1, 2)$.

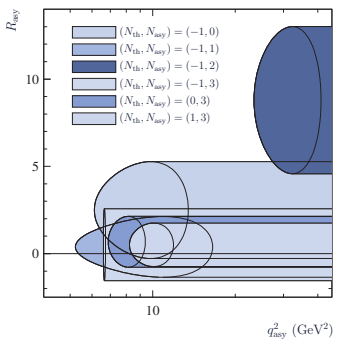

Figure 3. Asymptotic behaviors for each case $(N_{\rm th}, N_{\rm asy})$. The ellipses are centered at $(q^2_{\rm asy}, R_{\rm asy})$, with $R_{\rm asy} \equiv |G_E^\Lambda(q^2_{\rm asy})/G_M^\Lambda(q^2_{\rm asy})|$, and have the errors $\delta q^2_{\rm asy}$ and $\delta R_{\rm asy}$ as horizontal and vertical semi-axes, respectively. The right-hand side tails represent the error bands of the asymptotic constant values.

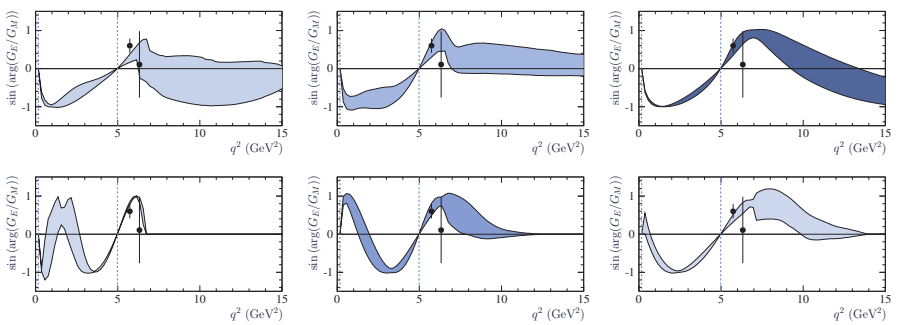

Figure 4. Sinus of the phase of the FF ratio with, from the top left to the down right: $(N_{\rm th}, N_{\rm asy}) = (-1, 0), (-1, 1), (-1, 2), (-1, 3), (0, 3), (1, 3)$. The color intensity is proportional to the occurrence probability, a darker color indicates a higher probability.

5.2 The phase of the ratio

Despite the inescapable fact that the direct knowledge of the phase determination is prevented by the periodicity of the sinus function, it could be somehow accessible by studying the behavior of the sinus itself as a function of q^2, from the theoretical threshold $q^2_{\rm th}$ on. Indeed, once the value at $q^2_{\rm th}$ is determined by means of the dispersive analysis, the value and its determination at a certain q^2 can be inferred by the number of oscillations undertaken by the

sinus function in the corresponding interval $(q^2_{\rm th}, q^2)$. It follows that the data on the sinus of the phase should describe a complete period, passing through the minimum value -1 and the maximum $+1$. This behavior unambiguously reveals the determination. This explicitly means that a set of data covering a reasonable q^2 range gives unique information on the physical determination of the phase. The results for the sinus of the phase $\arg\left(G^\Lambda_E/G^\Lambda_M\right)$ in the six cases under study, namely those with $\left(N_{\rm th}, N_{\rm asy}\right) = (-1,0)$, $(-1,1)$, $(-1,2)$, $(-1,3)$, $(0,3)$, $(1,3)$, are shown in Fig. 4. We notice that in the results with larger values of $\Delta N = N_{\rm asy} - N_{\rm th}$, most of the oscillations lie below the physical threshold and hence are not experimentally observable.

6 The charge radius of the Λ baryon

The knowledge of the analytic expression of the FF ratio in the whole q^2-complex plane allows us to compute static features of the Λ baryons. An example is the so-called charge root-mean-square radius, $\langle r^\Lambda_E\rangle$, which is defined by $\langle r^\Lambda_E\rangle^2 = 6\, dG_E(q^2)/dq^2\big|_{q^2=0}$, i.e., its squared value is six times the first derivative of the electric FF at $q^2 = 0$. The definition follows from the fact that, in the non-relativistic limit, the electric FF represents the Fourier transform of the spatial charge distribution of the baryon.

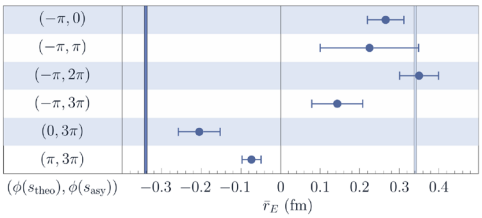

Figure 5. The points represent the normalized charge radii obtained in the six cases under consideration, whose $(N_{\rm th}, N_{\rm asy})$ pairs are reported on the left hand side of the picture. The symmetric vertical blue bars indicate the negative normalized neutron charge radius, on the left, and its reflection on the right.

In the case of a neutral baryon with non-vanishing magnetic moment μ, for which the electric and magnetic FFs are normalized as $G_E(0) = 0$, $G_M(0) = \mu \neq 0$, the charge radius can be defined in terms of the first derivative at $q^2 = 0$ of the ratio $R(q^2) = G_E(q^2)/G_M(q^2)$. In fact,

$$\left.\frac{dR(q^2)}{dq^2}\right|_{q^2=0} = \left.\left(\frac{1}{G_M(q^2)}\,\frac{dG_E(q^2)}{dq^2}\right)\right|_{q^2=0} = \frac{1}{\mu}\,\frac{\langle r^\Lambda_E\rangle^2}{6} \quad \Rightarrow \quad \langle r^\Lambda_E\rangle^2 = 6\mu \left.\frac{dR(q^2)}{dq^2}\right|_{q^2=0}.$$

This quantity depending on the signs of the magnetic moment and of the derivative can be either positive or negative. The neutron, for instance, has a negative squared charge radius, $\langle r^n_E\rangle^2 = -0.1161 \pm 0.0022$ fm^2 [14]. This is not a strange result. It can be explained in terms of the electric charge spatial distribution of the valence quarks, which is determined by their mean distance from the center of the neutron. The squared charge radius is negative when the two *down* valence quarks, bearing the negative charge, lie at a mean distance from the neutron center larger than the distance of the positively charged *up* quark. In order to have a better understanding of the linear extension of the baryon, we define a normalized charge radius, by taking the square root of the modulus of the squared charge radius to which we assign the original sign, i.e., $\bar{r}_E = {\rm Sign}\left[\langle r_E\rangle^2\right]\,\sqrt{\left|\langle r_E\rangle^2\right|}$. In the case of the neutron, it is $\bar{r}^n_E = -0.3407 \pm 0.0032$ fm. Figure 5 shows the obtained values of the normalized charge radius of the Λ baryon in comparison with the neutron one, indicated by the vertical dark blue bar. It is also reported its positive opposite, the light-blue bar on the right-hand side of the figure. It is found that in the most probable case, the one with $(N_{\rm th}, N_{\rm asy}) = (-1, 2)$, see Table 1, the quark configuration of the Λ baryon is the opposite of that of the neutron. The

negative charge, carried by the *down* and the heavy *strange* quarks, is concentrated at small distances. On the contrary, the second most probable result, that with $(N_{\rm th}, N_{\rm asy}) = (0, 3)$, having a probability of about half of that of case $(N_{\rm th}, N_{\rm asy}) = (-1, 2)$, has a negative squared charge radius at less than three standard deviations from that of the neutron. In summary, it is evident that, despite the capacity of the theoretical approach to restrict the set of possible configurations and solutions, more data are needed to reduce the multiplicity of the results for the charge radius.

7 Conclusions

A dispersive procedure is defined for analyzing the first precise experimental data on phase and modulus of the FF ratio G_E^Λ/G_M^Λ, obtained by the BESIII Collaboration [8]. This study is a first attempt to gain a deeper knowledge of the mechanism which is behind the electromagnetic coupling of the $\Lambda\bar{\Lambda}$ system in the time-like and space-like regions. The key point of this study is actually the space-time-like analytic connection of FFs. This connection implies that, as set forth by Levinson's theorem [9], the asymptotic value of the phase is directly connected to the number of zeros of the electric FF G_E^Λ lying in the space-like region. This kinematic region, characterized by negative q^2, due to the instability of the Λ baryon, is not experimentally accessible. Concerning the phase, in each of the six studied cases, reported in Table 1, there is a non-vanishing difference between the asymptotic and the threshold values, i.e., $\Delta\phi = \phi(\infty) - \phi(q^2_{\rm th}) = \Delta N\pi = (N_{\rm asy} - N_{\rm th})\pi \geq \pi$. This result indicates that the electric FF has at least one zero at a $q^2 \leq q^2_{\rm th}$, in agreement with its normalization to zero at $q^2 = 0$. The most probable solutions are those with $\Delta\phi = 3\pi$, with $(N_{\rm th}, N_{\rm asy}) = (-1, 2)$ and $(0, 3)$, see Table 1, and suggest that G_E^Λ has additional zeros with respect to the normalization. Such a property, if confirmed, is an interesting feature of G_E^Λ that, interpreted in terms of spatial charge distribution, could shed light on the dynamical mechanism underlying the electromagnetic coupling of the Λ baryon. We have discussed the possibility of observing the determination of the phase by studying the q^2-evolution of the sinus of the phase in connection with the modulus of the FF ratio in the framework of a dispersive procedure. As pointed out in Sec. 5.2, assuming that the ratio $R(q^2) = G_E^\Lambda(q^2)/G_M^\Lambda(q^2)$ is an analytic function in the whole q^2 complex plane, with the branch cut $(q^2_{\rm th}, \infty)$, the phase can only increase as q^2 goes from $q^2_{\rm th}$ up to the asymptotic threshold $q^2_{\rm asy}$. In this regard, the present experimental situation is quite promising, even though there is only one precise datum on the phase: $\sin(\phi_{\rm BESIII}) = 0.60 \pm 0.19$ at $\sqrt{q^2} = 2.396$ GeV, provided by the BESIII Collaboration. In fact, this phase is significantly different from zero, i.e., it has an increasing trend and the asymptotic threshold has not been reached yet. This is a clear indication that, by exploring a wider q^2 region, more oscillations of the sinus of the phase could be seen, from which the asymptotic value of the phase itself could be determined. The detailed description of this analysis is reported in Ref. [13].

References

[1] F. J. Ernst, R. G. Sachs, and K. C. Wali, Phys. Rev. **119**, 1105 (1960)
[2] M. P. Rekalo, Sov. J. Nucl. Phys, **1**, 760 (1965)
[3] C. Adamuscin, E. A. Kuraev, E. Tomasi-Gustafsson, and F. E. Maas, Phys. Rev. C **75**, 045205 (2007)
[4] A. Z. Dubnickova, S. Dubnička, and M. P. Rekalo, Nuovo Cimento A **109**, 241 (1996)
[5] E. Tomasi-Gustafsson, F. Lacroix, C. Duterte and G. I. Gakh, Eur. Phys. J. A **24**, 419-430 (2005)
[6] G. Fäldt, Eur. Phys. J. A **52**, 141 (2016)

[7] B. Aubert *et al.* [BaBar], Phys. Rev. D **76**, 092006 (2007)
[8] M. Ablikim *et al.* [BESIII], Phys. Rev. Lett. **123**, no.12, 122003 (2019)
[9] N. Levinson, Kgl. Danske Videnskab. Selskab, Mat.-Fys. Medd., **25** (9), 1-29 (1949)
[10] E. C. Titchmarsh, *Theory of Functions* (Oxford University Press, London, 1939)
[11] M. Abramowitz and I. A. Stegun, *Handbook of Mathematical Functions with Formulas, Graphs, and Mathematical Tables* (United States Department of Commerce, National Bureau of Standards, Washington D.C., 1972)
[12] C. W. Groetsch, *Inverse problems in mathematical sciences* (Vieweg, Braunschweig, 1993)
[13] A. Mangoni, S. Pacetti and E. Tomasi-Gustafsson, Phys. Rev. D **104**, no.11, 116016 (2021)
[14] R. L. Workman et al. (PDG), Prog. Theor. Exp. Phys. **2022**, 083C01 (2022)